Journal of Materials Chemistry B

Accepted Manuscript

ROYAL SOCIETY OF CHEMISTRY

www.rsc.org/materialsB

Rapid Prototyping of Chitosan-Coated Alginate Scaffolds Through the Use of a 3D Fiber Deposition Technique

Cristina Colosi[a], *Marco Costantini*[a], *Roberta Latini*[a], *Serena Ciccarelli*[a], *Alessandra Stampella*[c], *Andrea Barbetta*[a]*, *Mara Massimi*[b], *Laura Conti Devirgiliis*[c], *Mariella Dentini*[a]

[a]Department of Chemistry, Sapienza University of Rome, P.le A. Moro 5, 00185 Rome, Italy

[b]Department of Life, Health and Environmental Sciences, University of L'Aquila, 67100 L'Aquila, Italy

[c]Department of Biology and Biotechnology C. Darwin, Sapienza University of Rome, 00185 Rome, Italy.

*corresponding author: Andrea Barbetta,
Department of Chemistry, Sapienza University of Rome, P.le A. Moro 5, 00185 Rome, Italy
Tel.: +39 06 49913633
E-mail: andrea.barbetta@uniroma1.it

Abstract. Three dimensional, periodic scaffolds of chitosan-coated alginate are fabricated in a layer-by-layer fashion by rapid prototyping. A novel dispensing system based on two coaxial needles deliver simultaneously an alginate and calcium chloride solutions permitting the direct deposition of alginate fibers according to any designed pattern. Coating of the alginate fiber with chitosan and subsequent cross-linking with EDC and genipin assured the endurance of the scaffold in culture environment for a prolonged period of time. The cross-linking protocol adopted, imparted to the scaffold a hierarchical chemical structure as evidenced by Confocal Laser Microscopy and FTIR spectroscopy. The core of the fibers making up the scaffold is represented by alginate chains cross-linked by ester bonds only, the periphery of the fiber are constituted by an inter-polyelectrolyte complex of alginate and chitosan cross-linked in all pair combinations. Fibers belonging to adjacent layers are glued together by the chitosan coating. Mechanical behavior of the scaffolds characterized by different layouts of deposition was determined revealing anisotropic properties. The biocompatibility and capability of the scaffolds to sustain hepatocytes (HepaRG) cultures was demonstrated. Typical hepatic function such as albumin and urea secretion and induction of CYP3A4 enzyme activity following drug administration were excellent, thus proving the potentials of these constructs in monitoring liver specific function.

Introduction

Tissue engineering (TE)[1] combines biological and engineering expertise to provide artificially developed substitutes for tissues and organs, hence promoting repair and replacement therapies.

A key element involved in TE processes is the matrix or scaffold, which serves as a substrate or framework for cell growth, aggregation, and tissue development. Scaffolds must be porous and interconnected to allow cell migration during the colonization process and to allow the transport of nutrients and waste to and from cells. The internal porous architecture is mostly determined by the technology used for scaffold production and it can greatly influence the overall success of new tissue formation. Therefore, the controlled fabrication of scaffold structures is becoming increasingly important in modern approaches to regenerative medicine.

Among biomaterials, polymers, both natural and synthetic, are the mostly used for scaffold fabrication. Hydrogels, thanks to their high water content, have received a particular interest as scaffolding material since they resemble native extracellular environment, enhance fluid transport inside the matrix and possess mechanical properties similar to those of soft tissues.[2]

Rapid Prototyping (RP) is a manufacturing technology that has emerged since 2000 in TE for the fabrication of scaffolds with well-defined internal architecture.[3] Generally, in RP three motorized axis and a deposition system are used to lay down material in a layer by layer manner, generating a three-dimensional physical model from Computer-Aided-Design (CAD) data. This technology enables the tissue engineer to have full control over the design, fabrication and modeling of the scaffold being constructed, providing a systematic learning channel for investigating cell–matrix interactions. RP techniques are very specialized technologies in terms of material processability, and a great challenges is represented by the search of novel and effective deposition strategies to prototype hydrogel scaffolds.[4]

Among three Dimensional Fiber Deposition techniques (3DFD), two major methods have been devised for printing hydrogel-based scaffolds. In the first one, a concentrated solution of a biopolymer is deposited directly from a pneumatic syringe dispenser on an either static or moving platform. The shear-thinning experienced by the solution during the process of extrusion results in a fall in shear stress at higher extrusion pressures and is at the basis of the deposition of gel-like solution. Such an approach was exploited in the manufacturing of a semi-interpenetrated network of hyaluronic acid and dextran-methacrylate based scaffolds[5] and in the layered deposition of cell-laden hydrogel strands.[6] This method suffers from a lack in uniformity of the porous texture. Vertical pores are regular throughout the samples, whereas transversal pores tend to fuse together because of the relaxation downwards of the printed uncross-linked gel. Furthermore, the resolution of the printed scaffolds is rather poor. For instance, strand distance may vary from 0.5 to 2.5 mm.[6a]

As a consequence while it is valid for printing biopolymers and cells at the same time, this approach does not permit to exploit the full potential offered by RP in obtaining completely tailored scaffolds. A second major 3DFD technique employing biopolymers is represented by bioplotting where a solution of a biopolymer is printed in a coagulating bath. The key feature of this method is the 3D dispensing of liquids and pastes into a liquid medium with matched density. The plotting material leaves the nozzle and solidifies in the plotting medium after bonding to the previous layer. The liquid medium compensates for gravity and hence no support structure is needed.

This technique presents the inconvenience of a limited resolution, and fused horizontal pores have been mentioned in some cases. In addition, the 3D-Bioplotter technology is a time consuming technique due to the optimization of the plotting conditions for each different material[7] and highly water soluble materials cannot be processed with this technique.[8] We speculated that some of the above illustrated limitations could be overcome if the fiber-like, cross-linked (either physically or chemically) hydrogel making up the scaffold is formed simultaneously its extrusion. This approach can be realized practically by making recourse to a microfluidic-like dispensing system. In literature, examples of fibers produced via microfluidics are reported. For instance, a spider mimicking microfluidic device has been employed for the production of fibroin fibers.[9] Aligned collagen fibrils were deposited on planar substrates from collagen solutions streaming through a microfluidic channel system.[10]

The aim of this article is to illustrate a bioplotting approach based on a novel concept. Instead of printing in a coagulating bath or depositing a pre-gelled viscous solution we envisaged that by extruding at the same time the polymeric and the coagulating solution through the inner and outer needles, respectively, of a coaxial dispensing system it would be possible to deposit directly a solid filament. In this way the process of scaffold printing is greatly simplified since all the above reported limitations are bypassed. This approach relies on the ability of several biopolymers to undergo a rapid gelation when in contact with an appropriate chemical environment. For instance, acidified aqueous solutions of chitosan undergo gelation when exposed to basic solution.[7] Similarly, an aqueous solution of fibroin solidifies by re-establishing β-sheets junctions when exposed to methanol or ethanol.[11] Probably, the most popular and effective gelling biopolymer is alginate that when exposed to divalent cations, usually Ca^{2+}, instantaneously forms a physical gel by generating an egg-box network in which ions are caged between two alginate chains.[12] Furthermore, alginate has been found particularly useful in pharmaceutical and biomedical applications areas. Therefore alginate seems the optimal candidate to test the validity of the scaffold production system we are here proposing.

In the article we will show that the scaffolds produced may have practical applications. In the last decade there has been an increasing interest in the development of i*n vitro*-systems, especially 3D-culture systems on a chip-basis, for drug testing. There is a wealth of information on how cells confined in conventional 2D monolayer cultures differ substantially in their properties from cells cultured in a 3D configuration. Lacking the physical and chemical cues defining their natural *in vivo* microenvironment, cells in 2D culture differ substantially in their shape and organization, in contacts with neighboring cells, and in their physiology and metabolism from cells observed in more physiologically relevant 3D environments.[13] Thus, the drug evaluation process will stand to gain great benefits from the fairly accurate predictions of cellular responses displayed by 3D-engineered tissue models when exposed to the drugs of interest *in vitro.*

Liver toxicity is among the most common biological reasons for drug candidates to be pulled from clinical development, so it is important to be able to predict it. Even if a molecule does not harm the liver, that organ's detoxifying actions may harm the molecule, rendering potential drugs ineffective. Since the liver, and the hepatocyte in particular, is the main site of xenobiotic biotransformation and detoxification processes, and thus also of drug-induced toxicity in the body, cultures of liver cells provide a valid tool for systematic, repetitive and quantitative investigations in drug analysis, allowing also a significant reduction of the costs of preclinical drug development. Considerable attention has thus commonly paid to the establishment of relevant hepatic *in vitro* models. The HepaRG cell line was recently found to be a valuable human-hepatocyte *in vitro* model for investigating properties and potential effects of various drug compounds.[14] HepaRG cells are terminally differentiated hepatic cells that retain most characteristics of primary mature human hepatocytes. In contrast with other hepatoma cells such as HepG2, HepaRG not only express a range of P450 enzymes (CYP1A2, 2B6, 2C9, 2E1, 3A4) and respond to selective inducers of these enzymes, but also express other specific markers of adult hepatocytes, including nuclear receptors, drug transporters and phase II xenobiotic metabolizing enzymes.[15] In addition, results from recent studies show that HepaRG performance improve further when cultured in spheroids or in 3D organotypic cultures using scaffolds free systems.[16]

A drug screening construct to be effective needs to be reproducible and rely on a fabrication technology which is able to create highly structured 3D culture microenvironment with defined shape and position on the micrometer scale.

As a consequence an additional aim of this work is to demonstrate the efficacy of the printing process in creating scaffolds based on different geometrical webs and whether and how these influence the expression of liver specific functions in cultured differentiated HepaRG cells.

Experimental Section

Materials

Alginate (68% content in guluronic residues) was purchased from Fluka and purified by precipitation in ethanol and dialysed against distilled water before use. Its average molecular weight was determined by capillary viscosimetry (Ubbelohde capillary, Φ = 0.53 mm, for dilution sequences) using the viscosity measuring unit AVS370 (Schott-Gerate, Hofheim, Germany). Measurements were carried out on a solution of alginate in NaCl 0.01 M and in the elaboration of the experimental data the following Mark-Howink constants $K = 4.8\times10^{-6}$ dl/g, $a = 1.15$ were used. The average viscosimetric molecular weight (M_η) turned out to be 146 kg/mol. Chitosan, Low Viscous, was purchased from Fluka and used without further purification. Hexa-Methyl-Di-Silazane (HMDS) was purchased from Fluka. Calcium chloride, 1-ethyl-3,3-[3-(dimethylamino)propyl]carbodiimide hydrochloride (EDC), 2-(N-Morpholino)ethanesulfonic acid, 4-Morpholineethanesulfonic acid monohydrate (MES), were purchased from Sigma. Genipin was purchased from Wako.

Experimental Set-Up

The experimental set-up used to fabricate alginate scaffolds has been assembled in our laboratory. It consists of three-motorized precision linear stages (Micos): X-Y movement is associated with the deposition plane, Z movement is associated with the extrusion system. Deposition paths are generated using a custom Matlab algorithm in which fiber position (spacing and orientation) and scaffolds macroscopic dimensions are set. The extruder is constituted by two needles, assembled one inside the other and fixed with silicone glue (Figure 2.a). The internal needle (Hamilton) has a 26 G dimension (ID = 260 μm, OD = 470 μm) and supplies alginate solution; the external needle (Fishman) has 19 G dimension (ID = 690 μm, OD = 1070 μm) and supplies calcium chloride solution. The internal needle protrudes out from the external one of approximately 500 μm. Both flows are controlled volumetrically by means of two microfluidic pumps (Harvard Apparatus).

Characterization of the fibers deposited with the coaxial-needles system

To characterize the deposition step using the coaxial needles system, the dimension of the fibers in scaffolds produced at different flow rates of alginate (Q_{al}) and calcium chloride (Q_{ca}) and at different velocities of the deposition plane (*FR*, *feed rate*) (Figure 1) were measured using light microscopy images and ImageJ software. Before acquiring microscopy data, samples were kept in the cross-linking solution used during the printing process ($CaCl_2$ 0.22M, MES 0.2M, PH=4.5) for 24h to let them reach the swelling equilibrium. These measurements were compared with a simple theoretical model in which the fibers are supposed cylindrical and their dimension is predicted using a volumetric equivalence:

$$Q_{al} = FR \times A_f$$

$$A_f = \frac{d^2}{4} \times \pi$$

where A_f and d are the diameter and area of the circular section of the cylindrical fiber, respectively (Figure 1).

Scaffold production and crosslinking

Purified alginate was dissolved in distilled water at a concentration of 4% w/v. Calcium chloride was dissolved in distilled water at a concentration of 0.22 M. The two solutions were put in plastic syringes. Printed scaffolds were designed to have a 10mm×10mm×1mm or 5mm×5mm×5mm total dimension. Each layer is formed of parallel fibers and the orientation of fibers in adjacent layers was set at 0-90° for the squared pattern, 0-60°-120° for the hexagonal pattern. Fiber spacing was set to 200 μm. Fiber diameter was adjusted to 130 μm imposing equal alginate and calcium flow rates with the use of syringe microfluidic pumps ($Q_{al} = Q_{ca} = 5$μl/min) and the substrate speed was set to 235 mm/min. Layer height was set to 90% of the fiber diameter in order to favor surface contact between consecutive deposited layers. At the end of the 3DFD process, prototyped alginate scaffolds were immersed in a 2M calcium chloride aqueous solution for 24h before proceeding with the coating step with chitosan. Chitosan and calcium chloride were dissolved in 0.2M MES buffer (pH = 4.5) at a concentration of respectively 1% w/v and 0.1M. Scaffolds were immersed in the chitosan solution for 24h, and then cross-linked in an ethanol-water mixture (8 : 2) containing genipin (1% w/v) and EDC (one third of total alginate weight, alginate : EDC = 3 : 1) for 48h. Finally, scaffolds were dialyzed against 1M sodium chloride solution to rapidly remove calcium ions and EDC and then against distilled water until reaching its nominal conductivity.

Scaffold coding system.

In order to identify the scaffolds obtained in the various steps of cross-linking and to distinguish between those characterized by different geometries of printing, a simple coding system was adopted. Scaffolds made of calcium-alginate were indicated as Ca-Alg. Alginate scaffold cross-linked with EDC were indicated as Alg_{EDC}. The code for alginate scaffold cross-linked with EDC, coated with chitosan and cross-linked with EDC and genipin is Alg.Chit. To distinguish scaffolds printed according to a square or hexagonal geometry, the suffix s or h was added to Alg.Chit ($Alg.Chit_s$, $Alg.Chit_h$).

Scaffold Characterization

Prototyped and cross-linked scaffolds were visualized by means of scanning electron microscopy (LEO 1450VP, Oxford Instruments), stereo-microscopy (Leica Stereozoom S8 APO equipped with a EC3 camera) and confocal microscopy (Zeiss LSM 510, Carl Zeiss). Before SEM

characterization, samples were dried using increasing graded ethanol/water mixtures (from 30% to 100% ethanol), and then in increasing graded HMDS/ethanol mixtures (from 30% to 100% HMDS), and were finally gold-sputtered (SEM COATING UNIT 953, Agar Scientific). For confocal imaging, the fluorescence of the genipin bound to chitosan was exploited. Samples immersed in water were excited with a 405 nm light source and transmitted light was detected. A scansion depth of 300 μm or 30 μm was used to visualize respectively many layers of the scaffold or highlight the internal structure of a single fiber.

FTIR spectroscopy

The connectivity between alginate-alginate, chitosan-chitosan and alginate-chitosan networks in the printed hydrogels was examined using Fourier Transform IR spectroscopy.

The IR analysis of scaffold fragments was carried out, collecting a sequence of spectra by means of a Thermo Scientific Nicolet 6700 FT-IR equipped with a Golden Gate to perform measurements in Attenuated Total Reflection (ATR) mode. The sequence of spectra was acquired in the absorbance mode in the 800–2000 cm^{-1} range, by executing 200 scans at 4 cm^{-1}resolution.

Hydrogel specimens were oven dried at 80 °C for 4 hours prior to analysis. The spectra were processed using Happ-Genzel apodization, ATR correction, smoothing and baseline correction algorithms. Deconvolution of spectra was carried out by means of PeakFit 4.12. The second and fourth derivatives of the input spectra were examined in order to reveal the presence of hidden peaks.

Mechanical testing

The compressive stress-strain measurements were performed on the water swollen printed hydrogels (Alg.$Chit_s$ and Alg.$Chit_h$) using a Instron 3365, equipped with a 10 N load cell. The cubic gel samples of 0.5 cm of edge were set on the lower plate and compressed at a strain rate of 1.2 mm/min to 70% deformation by the upper plate, which was connected to the load cell. Measurements were carried out at room temperature. Elastic moduli were derived from the regression of the linear portion of stress–strain curves. Each measurement was performed in quintuplicate. Results are reported as the mean±standard deviation.

Cell culture

The terminally differentiated human HepaRG cells (Life Technologies™ , Gran Island, NY, USA) were suspended in Williams' Medium E supplemented with 10% fetal bovine serum, 1% GlutaMAX™-I, 100 U/mL penicillin, 5 μg/ml of Insulin, 25 μg/ml of streptomycin. The cell seeding procedure was modified from that described previously [32b]. Briefly, 5×10^5 cells in 40 μl of medium were loaded into the UV sterilized biomaterials. Scaffolds with the entrapped cells were

incubated at 37°C in a humidified atmosphere of 5% CO_2 for 5 h to allow cell settlement. After this incubation period, fresh medium was added to each well. In parallel experiments, cells, suspended in the same medium, were seeded on Collagen I-coated plates (3×10^5 cells/cm^2) and cultured in monolayer.

Scanning Electron Microscopy (SEM)

Cell-seeded materials were rinsed with cultured medium and fixed with 2% glutaraldhyde in 0.1 M Na-Cacodylate buffer with 0.1 M sucrose for 12 h. After treatment with 1% tannic acid in 0.15 M Na-Cacodylate buffer for 1 h, the samples were dehydrated in ethanol solution (from 70% to 100%). The samples were then immersed in 100% hexamethyldisalazane (HMDS) for 3 min, dried and mounted on aluminum stubs and gold-sputtered with a thin layer of gold. Specimens were finally examined using an XL 30 CP (Philips) SEM.

Viability/cytotoxicity assays.

Cell viability was determined throughout the culture by means of a MTS assay. 20 µl of Cell Titer 96 AQueous One Reagent (Promega, Madison, WI, USA) were added to the cell-seeded scaffolds cultured in 100 µl of complete medium and incubated for 1 h a 37°C. MTS [3-(4,5-dimethylthiazol-2-yl)-5-(3-carboxymethoxyphenyl)-2-(4-sulfophenyl)-2H-tetrazolium] bio-reduced product was quantified by absorbance at 490 nm (GLOMAX, Promega). Values obtained in the absence of cells were considered as background. A standard curve was assessed to convert 490 nm O.D. values to the number of viable cells, using cell densities ranging from 0 to $4x10^5$ cells.

To determine the extent of cell damage and toxicity, the release of lactate dehydrogenase (LDH) by impaired cells was quantified in supernatants and compared with the LDH content of the total cell lysates. A LDH-cytotoxicity assay kit (BioVision Inc., Mountain View, CA) was used according to the manufacturer's instructions. Before the assay, wells were washed with PBS and fresh medium was added; after 24 h, this medium was withdrawn and 100 ml aliquots were assayed. Absorbance was measured at 450 nm using a microplate reader. High absorbance equating to 100% LDH release was obtained by treating the entrapped cells with the lysis solution provided with the kit. Values obtained in the absence of cells were considered as background. Each experiment was performed in triplicate.

Albumin secretion Assay

Enzyme-linked immunoassorbent assay (ELISA) Quantitation kit (Bethyl Laboratories Inc., Montgomery, TX, USA) was used to measure albumin levels during the culture period (at 2, 6, 9 and 15 days). Before the assay, wells were washed with PBS and fresh medium was added; after 24 h, this medium was withdrawn and aliquots were used for the specific albumin secretion assay. Human albumin was used to establish the standard curve. The levels of albumin measured at each

time point were normalized to the cell number obtained by MTS assay. Each experiment was performed in triplicate.

Urea secretion Assay

Urea secretion was determined by a colorimetric test using the QuantiChrom Urea Assay Kit (BioAssay Systems, Hayward, CA) designed to measure urea directly in biological samples. The intensity of the color measured is directly proportional to the urea concentration in the sample. Urea secretion was measured at 450 nm at different intervals of culture (2, 6, 9, 15 days). Twenty-four hours before the assay, wells were washed with PBS and fresh medium was added; at the time of performing the test, this medium was withdrawn and aliquots were used for the specific urea secretion assay. The levels of urea measured at each time point were normalized to the cell number obtained by MTS assay and expressed as $\mu g/10^5$ viable cells/24 h. Each experiment was performed in triplicate.

CYP3A4 assay

CYP3A4 activity was measured using a luminescent method (P450-Glo™ Assay, Promega) following the manufacturer's instructions, as detailed elsewhere.[17] Entrapped cells were treated for 72h with Dexamethasone 10^{-4}M to induce the CYP3A4 enzyme activity. Dexamethasone was dissolved in dimethyl sulphoxide (DMSO), whose final concentration never exceeded 0.1% (v/v). Dishes containing the corresponding amount of vehicle alone (DMSO) were considered as controls. After treatment, medium was replaced with fresh medium containing luminogenic CYP3A4 substrate 1:40 (Luciferin-PFBE) and incubated for 3½ h. After incubation, 25µl of medium was combined with 25µl of Luciferin. Detection reagent and luminescence was read after 20 min at room temperature. Luminescence background was calculated by adding the luminogenic substrate to medium without cells. Values obtained after 6, 9, 15 days of culture were normalized to the cell number obtained by MTS assay and expressed as $RLU/10^5$cells. Each experiment was performed in triplicate.

Statistical Analysis.

The student *t*-test was used to analyze the statistical significance of the data. Differences with a *p* value <0.05 were considered significant.

Result and Discussion.

Three-Dimensional Fiber Deposition (3DFD) is probably the most simple and popular technique within Rapid Prototyping, in which a 3D object is created by the horizontal deposition of fibers, layer upon layer. Usually, this translates into a rougher approximation of the 3D computer-generated models when compared to other RP techniques, like stereolitography or 2-photon

polymerization, but this limitation is balanced by a much simpler and cost-effective hardware set-up.

In this work we present a Three Dimensional Fiber Deposition (3DF) strategy for the production of alginate hydrogel scaffolds. In contrast to so far developed systems for the 3D deposition of alginate fibers[8] that generally uses proper plotting medium to obtain the gelification of the polymer or deposits pre-gelled alginate[6], we induce the physical gelation of alginate simultaneously with its extrusion using two coaxial needles (Figure 3.a): the internal one is fed with an alginate aqueous solution, the external one with a calcium chloride aqueous solution. As soon as the two flows come into contact at the tip of the dispensing system, the biopolymer solution undergoes gelation. This gel adheres to the deposition plane and by moving the dispensing system, a gelled alginate fiber is laid down, similarly to wet-spinning process . The calcium solution, continuously provided through the external needle, wets the scaffold preventing its drying during the time of deposition.

The dimension of the fiber depends on the imposed volumetric flows for the alginate and calcium chloride solutions and on the speed of movement of the extruder (Figure 1). Predicting fiber dimension for different values of the control parameters is crucial for the generation of the codes of movement for the robotic dispensing system and for the subsequent success of the printing process. In Figure 2 the dependence of fiber diameter (d) on FR and Q_{ca} is reported, while Q_{al} was kept constant at 5μl/min. These measurements show that the diameter of the deposited fibers decreases from that predicted by the volumetric equivalence as the outer flow of $CaCl_2$ is increased. An excessive outer flow can, on the other hand, disturb the deposition of the first layers of the scaffold, and for Q_{ca} > 10 μl/min the fidelity of reproduction of the designed scaffold rapidly decreases. As shown by Figure 2, with the alginate concentration used and dimension of the needles indicated, the range of fiber diameter obtained spanned between 120-260 μm. From these experiments also emerged that the diameter of the internal needle through which alginate is supplied to the extruder represents an intrinsic superior limit for the dimension of deposited fibers. With our system, a decrease of FR or Q_{ca} in order to obtain fibers bigger than 260 μm produces creased or undulating rather than stretched out fibers, often causing the failure of the printing process.

As far as the inferior limit of fiber dimension is concerned, we deposited fibers with a maximum velocity of the deposition plane of 385 mm/min, that led to fibers of 100μm. This does not represent a strict inferior limit to fiber dimension, as an increase of either FR or Q_{ca}, or a decrease of Q_{al} may induce to some extent a further reduction of the fiber dimension. If the dimension of the fiber is too small with respect to the internal needle, a loss in accuracy and reproducibility may occur as a consequence of the possible unwanted contact between the needle and the deposited structures during the printing process. It is also worth noticing that the dimension of the fiber is independently

correlated to the deposition speed and the calcium outer flow: fiber produced at Q_{al} = 3μl/min, Q_{ca} = 3μl/min, *FR* = 140 mm/min, have the same dimension as fibers produced at Q_{al} = 5μl/min, Q_{ca} = 3μl/min, *FR* = 235mm/min (Q_{al}/FR = cost, *d* = 160 μm).

The described co-flowing extrusion system is mounted on a motorized Z axis while glass slides, used as deposition substrates, are moved in the X-Y direction. A computer generated path designs the porosity and architecture of the scaffold by defining the distance between adjacent fibers and the direction of deposition for each layer, until a three-dimensional porous material of desired macroscopic dimension is obtained, as shown in Figure 3.b. In Figure 3.c,d,e a few examples of different patterns of deposition are provided. As it can be seen the process of writing is very precise and lead to scaffold with a neat structure. The deposition of fibers proceeds in a continuous fashion, and as it is clear in Figure 3.e and videos provided in the Supporting Information, it maintains its fidelity also when it rapidly changes direction.

At the end of the prototyping step, a fibrous scaffold of ionically cross-linked alginate was obtained. Since the interaction between alginate and calcium is of physical nature, it is reversible and, in particular, destabilization of the egg-box structure occurs when the scaffold is exposed to solutions containing monovalent cations.[18] Furthermore, since gelation of the alginate fiber induced by exposure to calcium ions starts from the outer shell of the filament of solution extruded, the fiber deposited is wrapped by a sheet of calcium ions which hinder the interaction and bonding among fibers belonging to successive planes. A relatively high concentration of Na^+ is present in common cell culture medium, thus the gelation process induced by calcium ions during the prototyping of the scaffold is insufficient to produce chemically stable scaffolds suitable for cell seeding. In particular, it experimentally emerged that after being soaked in RPMI-1640 cell culture medium, the scaffolds firstly swelled (Figure 4.b), then lost their ordered structure because of the detachment of consecutive layers (Figure 4.c) and finally the fibers dissolved (Figure 4.d).

To overcome this problem, we decided to proceed with a chemical post-cross-linking of alginate preceded by the deposition of a chitosan coating on the scaffold fibers. Chitosan is another naturally derived polysaccharide very used in TE which is a linear copolymer of D-glucosamine and *N*-acetyl-D-glucosamine.[19] It has been proven to be biodegradable, biocompatible, non-antigenic, non-toxic, bioadhesive, anti-microbial, bioactive and to have haemostatic capacity.[20] It is a positively charged biopolymer that, through electrostatic interaction, can be deposited on negatively charged alginate fibers by simply soaking the alginate scaffold in a chitosan aqueous solution. The formation of an inter-polyelectrolyte network limits fiber swelling, and the deposited chitosan coating reinforces the attachment between consecutive layers. Moreover, chitosan/alginate hybrids have been shown to induce a more pronounced cell adhesion with respect to pure alginate[21] or

chitosan[22] scaffolds, therefore this coating step should also improve cellular affinity for the substrate. In order to further improve the stability of the scaffolds produced, covalent cross-linking was employed to strengthen the chitosan membrane using a naturally-derived cross-linker, genipin (Figure 4.e,f).[23] In the cross-linking reaction, genipin, a small molecule, can freely diffuse through the alginate-chitosan complex membrane and interact with the chitosan bound to the alginate gel. The reaction of genipin occurs according two different pathways. The first and faster one involves a nucleophilic attack of the amino groups of chitosan on the genipin olefinic carbon atom at C3 to form an intermediate aldehyde group, followed by the opening of the dihydropyran ring. The resulting aldehyde group is subsequently attacked by the secondary amine group formed in the first step of the reaction step. In this way a heterocyclic compound of genipin linked to the glucosamine residue of chitosan is thereby formed.[25] In the second one, the ester group of genipin is attacked by the amino groups of chitosan leading to the formation of secondary amide linkages. Eventually a three-dimensional interpenetrating network structure is created within the fiber membrane. The fluorescence behaviour of genipin bound to chitosan was exploited to inspect the effective coating of the alginate scaffold fibers. Imaging of the scaffold on the whole and of the single fibers through CLSM analysis supported this hypothetic structure. From Figure 5.a,b, it is clearly visible that chitosan uniformly covers the scaffolds. Genipin reacts selectively towards primary amines[26] of chitosan while is inert towards alginate, as a consequence the presence of a bright external layer (Figure 5.c) is indicative of the formation of new fluorescent chitosan-genipin conjugates and visually demonstrates the presence of a shell-like cross-linked membrane of approximately 40 μm thickness (Figure 5.d) surrounding the fiber core. The intensity of the fluorescence in the fiber external layer is directly proportional to the degree of cross-linking and to the distribution of the chitosan coating in the membrane. The stronger the fluorescence, the more genipin-chitosan conjugates were formed, and thus, the higher cross-linking degree in the chitosan coating was attained. As it is evident from Figure 5.d the fluorescence signal is stronger at the external border of the fiber and tend to fade out proceeding towards the center. This may be due to restricted diffusion of chitosan into the alginate core blocked by initial chitosan binding and/or a higher degree of cross-linking at the external border of the membrane where more chitosan was deposited. In any case, this treatment confers to the scaffold the desired stability in culture medium as evidenced by Figure 4.e,f.

Since as evidenced by CLSM, chitosan coating and cross-linking by genipin involves only the outer shell of the fiber and leaves unaltered the core made of alginate, in order to obtain cross-linking throughout the whole of the fibers and to enhance the cross-linking density through the creation of additional bridges among the different macromolecular pairs (alginate-alginate, alginate-chitosan

beside chitosan-chitosan) we added EDC to the reaction medium (ethanol:H_2O = 80/20), besides genepin.

The effective occurrence of the various type of cross-linking among the macromolecular pairs was investigated by mean of IR spectroscopy. Since the spectrum of the final scaffold is of difficult interpretation due to the complexity of the material from a compositional point of view, we have recorded the spectra of the scaffold at each stage of cross-linking. Furthermore, spectra analysis was facilitated by carrying out the deconvolution of partially overlapped peaks,

In Figure 6.A the spectrum of the scaffold directly produced by the RP machine i.e. alginate physically cross-linked with calcium (Ca-Alg) is displayed. Typical bands relative to the symmetric and asymmetric stretching of the carboxylate groups at 1581, 1412 and 1026 cm^{-1} and skeletal vibrations of the C─O─H and C─O─C at 1300, 1244 and 1088 cm^{-1} are clearly discernable in the deconvoluted spectrum. In Figure 6.B the spectrum of calcium-alginate cross-linked with EDC (Alg_{EDC}) in ethanol/water = 80:20 is reported. The additional bands appearing at 1666 cm^{-1} provides clear evidence of the formation of ester linkages among alginate chains. Furthermore, there is an evident increase of the intensity ratio of the peaks positioned at 1088 and 1028 cm^{-1} in Alg_{EDC} spectrum with respect to Ca-Alg one. The O─C─C band of ester group occurs in fact in the 1150-1030 cm^{-1} range. The percentage of cross-linking can be quantified from the ratio of the area of the peak at 1666 cm^{-1} and the sum of the areas of the peaks at 1666 and 1589 cm^{-1}. It turns out that the degree of cross-linking of Alg_{EDC} is 12%. Cross-linking operated by EDC involves alginate chains within a single fiber but is not effective in bonding different fibers to each other. This causes the detachment of the fibers in culture medium which is rich of sodium ions, among the others. This outcome induced us to coat the alginate scaffold with chitosan and to carry out a second and third cross-linking process by using EDC and genipin at the same time. Again, to help in the interpretation of the spectrum of the final scaffold, we proceeded first in a comparative analysis of the IR spectra of native chitosan and a genipin-cross-linked chitosan scaffold produced by gas-in-liquid foam templating[27] as shown in Figure 6.C,D. The C=O stretching absorption band of the new formed amide at 1649 cm^{-1} [29] overlaps with amide I absorption band of chitosan (1655 cm^{-1}) and makes it become broader. A new broad peak that appeared around 1419 cm^{-1} after cross-linking by genipin, indicated the presence of ring-stretching of heterocyclic amine. The C–N stretching of amide III of chitosan at 1233 cm^{-1} shifted to 1260 cm^{-1} after cross-linking by genipin. New bands appearing at 1703, 1201 and 1236 cm^{-1} are due to the conjugated acetate present in genipin. Bands at 1594 and 1379 cm^{-1} are due to the bending vibration of $–NH_2$ and the stretching absorption of C–N. The apparent absence of the C=C stretching in cyclic structure of genipin at 1628 cm^{-1} allows

presuming that reaction of the amino groups of chitosan with genipin occurs mainly on the olefinic group.[29]

The spectrum of Alg.Chit scaffold is very complex but bands characteristic of the alginate-chitosan complex are discernable. A broad band at 1583 cm^{-1} with a prominent shoulder at 1523 cm^{-1} as well as a band at 1406 cm^{-1} can be observed. The two main bands are assigned to the carbonyl vibrations of the carboxylate groups of alginate. The broadness of these bands arises from overlapping bands from the partly protonated chitosan moieties and the prominent shoulder corresponding to the 1535 cm^{-1} band seen in the chitosan reference scaffold. The peak at 1716 cm^{-1} is due to the carbonyl vibration of the carboxylate group in the protonated form. When chitosan was dissolved in hydrochloric acid and put into contact with the alginate scaffold in water, one reaction that takes place is the protonation of alginate.[30] A related band is that at 1300 cm^{-1} which refers to the stretching vibration of C─O of the COOH group.

The groups of bands in the region between 900-1150 cm^{-1} are clearly the overlapping of the skeletal vibrations of the two polysaccharides. The characteristic peak of genipin at 1201 cm^{-1} is still clearly visible.

The picture that emerges from the combined analysis of the CLSM images and IR data is as follows: the whole of a fiber is represented by a network of alginate chains auto cross-linked by ester bonds. The outer shell of the fiber (thickness ~ 40 μm), as evident from CLSM images (Figure 5) and IR data, is composed by an interpenetrating polymer network of alginate-chitosan chains cross-linked by amide bonds and chitosan-chitosan chains cross-linked by genipin bridges. On a higher length scale, fibers making up the scaffold are glued together by the genipin cross-linked chitosan network.

From SEM micrographs of Figure 7b,c and 7e,f, it is evident that the printed scaffolds exhibit an anisotropic morphology. Fibers are oriented horizontally and have a 200 μm spacing in the x-y plane, and a 120 μm spacing in the z direction (layer height). This should translate into direction dependent mechanical properties which is an usual characteristic of many tissues in the human body. Compressive testing was conducted on $Alg.Chit_s$ and $Alg.Chit_q$ in a perpendicular (⊥) and parallel (\\) direction (Figure 8.a) with respect to the deposition plane obtaining two distinct values of the Young modulus (denoted as $E_{\perp}$ and $E_{\backslash\backslash}$, respectively). The compressive stress/strain curves of $Alg.Chit_s$ are displayed in Figure 8.b. As it can be observed, the ⊥ curve exhibits a linear region for a very extended range of strain (up to 50%) and beyond this limit it tends to rise moderately. The correspondent value of $E_{\perp}$ is 23.3 kPa (Table 1). This mechanical behavior matches well with the cross-sectional morphology of the scaffold. In the ⊥ direction, spacing among fibers (Figure 7c) is relatively small and upon compression, bending of fibers is relatively less pronounced. The modest

rise observed above 50% strain is ascribed to scaffold densification. A totally different behavior can be observed for the curve describing compression in the \\ direction. In such a case, spacing among fibers (Figure 7b) is more relevant and the stress/strain curve consists of three different regions. The first one is a linear region (up to approximately 5% deformation, insert of Figure 8) with a first increase with stress, which corresponds to cell edge bending. The Young's modulus is calculated from the linear slope of the stress–strain curve in the first region and as reported in Table 1, is about three time higher than $E_{\perp}$. This because half of the fibers are directed parallel to the applied force and oppose with the as highest efficacy as possible to the applied stress. The second one is a stress plateau region, which corresponds to progressive cell collapse by elastic buckling. When the opposite cell walls come into contact, cell collapse ends. This is the third regime, called densification, which denotes a collapse of the cells throughout the material. Upon compression, the stiffness of the cellular material increases and converges towards the stiffness of the base material.

The mechanical behavior of Alg.Chit$_h$ (data not shown) is the same for what concerns compression in ⊥ direction and it is less pronounced in the \\ one as evidenced by Young moduli (Table 1) since in this case only one third of the fibers are parallel to the applied force and its nominal porosity is very similar to that of Alg.Chit$_s$.

Cell Studies

Both squared and hexagonal scaffolds were seeded with HepaRG cells. Cells showed a favorable initial colonization of the scaffolds and appeared well organized in the three-dimensional space. Scanning electron micrographs of cells cultured on squared (Figure 9.a,b,c) and hexagonal (Figure 9.d,e,f) scaffolds showed a homogeneous distribution of cells and a high level of adhesion to the fibers within the scaffolds. Cells showed a good ability to colonize and survive on both these biomaterials; they adhered firmly to the materials and not only to each-others, spreading on the fibers, rather than promoting the formation of spheroids that are often observed with more proliferating cell types, such as HepG2 cells.[31] Due to their differentiate phenotype, HepaRG cells are strictly anchorage-dependent; after adhesion, they spread on fibers and merge forming flat multilayer aggregates, which remind the hepatic cords. In fact, due to oxygen and nutrient diffusion difficulties, spheroid culture could be limited in its ability to be used for long-term cultures, thus making the proposed system more attractive. Cells also showed high level of vitality, as revealed by MTS test (Figure 10.a), suggesting a good capacity of the scaffolds to allow hepatocyte entrapment and maintenance.

To evaluate indirectly the toxicity of these scaffolds, lactate dehydrogenase (LDH) leakage was monitored in both cell supernatant and total cell lysate and the ratio of released and total LDH was calculated (Figure 10.b). Cells after the first two days of culture, maintained good viability

throughout the entire time, with very low LDH leakage ratio, considered satisfactory for this cell type.[32] The somewhat higher levels of LDH leakage into the medium observed at the first two days of culture are probably due to detachment of cells that were not firmly adherent to the material. Therefore, the subsequent decreased levels of LDH leakage in combination with the high number of viable cells, revealed by MTS assay, exclude possible adverse effects of biomaterials against entrapped hepatocytes.

The good efficiency of HepaRG cells cultured in these scaffolds was evaluated by measuring the levels of albumin secretion and urea production, typical functions of well differentiated hepatocytes (Figures 11.a,b). The levels of these products were considerably high, with a maximum reached between 6 and 9th day for both the hexagonal (Alg.Chit$_h$) and the squared (Alg.Chit$_s$) morphology. Cells grown on both kind of scaffolds showed better hepato-specific activities than cells in monolayer. Similar results were obtained with cells cultured on Alg.Chit$_h$ and on Alg.Chit$_s$, suggesting that both morphologies could represent adequate support and optimal conditions for the maintenance of hepatocyte functions.

HepaRG cells, as said above, express a wide range of P450 enzymes and respond to selective inducers of these enzymes. Within these new scaffolds, cells are expected to be in an ideal condition to perform detoxification processes. This prompted us to assess the responsiveness to CYP3A4 inductors of the HepaRG cells entrapped into these scaffolds. The activation degree of CYP3A4 enzyme by 10^{-4} M dexamethason (DXM) was very high with respect to monolayer cell cultures (Figure 12) at each time point examined. The induction was not significantly different in the two kinds of scaffolds.

These data are in agreement with the morphological observations at the optic and scanning electron microscopy and demonstrate that both kinds of scaffolds provide an agreeable environment to support hepatocyte attachment, growth and performance, thus promising to become a valuable *in vitro* system on which to study liver specific functions and metabolism or to be used as a tool for the screening of new drugs or potentially toxic substances.

Conclusion

The use of a coaxial dispensing system coupled with a RP machine permitted the fabrication of alginate scaffold with an ordered structure and a fully interconnected morphology. The post-treatment of the scaffolds, consisting of coating the assembly of fibers making up the scaffold with a sheet of an interpolyelectrolyte complex with chitosan and its subsequent cross-linking with EDC and genipin, assured their structural stability in culture medium for a prolonged period of time. The

scaffolds based on different deposition layout are characterised by anisotropic mechanical properties.

Preliminary culture tests of a well differentiated human hepatocyte line showed that the scaffolds were biocompatible and were densely populated from seeded cells. The high level of albumin and urea secretion coupled with the high responsiveness to the induction of CYP3A4 enzyme make this system an attractive tool for testing the toxicity of new drugs.

The present dispensing technique has the potentials of printing materials with sophisticated and unmet hierarchical structures. For instance, one can imagine to connect the inner needle of the dispensing system to the outlet of a microfluidic device which can be used to generate an oil-in-water emulsion. If the dispersed phase is represented by either a non-polymerizing or polymerizing phase and the external phase by an aqueous solution of a gelling biopolymer it is possible to obtain either printed materials with porous fibers or a composite material in which individual fibers are made by an inner thread of a hydrophobic polymer and an outer sheet of a hydrophilic polymer obtaining in this way the double target of reinforced materials and a hydrophilic and biocompatible surface. Furthermore, the method of scaffold manufacturing through fiber layering presented here is compatible with different chemistries. A promising approach is represented by click chemistry which, in appropriate conditions, is an almost instantaneous reaction that can be utilized with many properly functionalized biopolymers.

Acknowledgements

The authors thank “Sapienza” University of Rome (Ateneo funds) for financial support.

References

(1) E. Lavik, R. Langer, *Appl. Microbiol. Biotechnol.* **2004**, *65*, 1-8.

(2) a) J. L. Drury, D. J. Mooney, *Biomaterials* **2003**, *24*, 4337-51; b) S. Van Vlierberghe, P. Dubruel, E. Schacht, *Biomacromolecules* **2011**, *12*, 1387-1408.

(3) a) W.-Y. Yeonga, C.-K. Chuaa, K.-F. Leonga, M. Chandrasekaran, *TRENDS in Biotechnology* **2004**, *22*, 643-52; b) D. W. Hutmacher, M. Sittinger, M. V. Risbud, *TRENDS in Biotechnology* **2004**, *22*, 354-62; S. J. Hollister, *Nature Materials* **2005**, *4*, 518-24; c) S. M. Peltola, F. P. W. Melchels, D. W. Grijpma, M. Kellomäki, *Annals of Medicine*, **2008**, *40*, 268-80; F. P.W. Melchelsa, M. A. N. T. Domingosc, J. Kleina, J. Maldaa, P. J. Bartoloc, D. W. Hutmacher, *Progress in Polymer Science*, **2012**, *37*, 1079-1104.

(4) a) S. A. Park, S. H. Lee, W. D. Kim, *Macromolecular Research* **2011**, *19*, 694-98. b) A. Ovsianikov, A. Deiwick, S. Van Vlierberghe, P. Dubruel, L. Moller, G. Dragerand, B. Chichkov, *Biomacromolecules* **2011**, *12*, 851-58 .c) T. H. Ang, F. S. A. Sultana, D. W. Hutmacher, Y. S. Wong, J. Y. H. Fuh, X. M. Mo, H. T. Loh, E. Burdet, S. H. Teoh, *Materials Science and Engineering C* **2002**, *20*, 35-42 d) T. Billiet, M. Vandenhaute, J. Schelfhout, S. Van Vlierberghe, P. Dubruel, *Biomaterials* **2012**, *33*, 6020-41.

(5) L. Pescosolido, W. Schuurman, J. Malda, P. Matricardi, F. Alhaique, T. Coviello, P. Rene van Weeren, W. J. A. Dhert, W. E. Hennink, T. Vermonden *Biomacromolecules* **2011**, *12*, 1831–1838.

(6) a) N. E. Fedorovich, J. R. De Wijn, A. J. Verbout, J. Alblas, W. J. Dhert, *Tissue Eng. Part* A **2008,** *14*, 127-33. b) G. Vozzi, A. Previti, D. De Rossi, A. Ahluwalia, *Tissue Eng.* **2002**, *8*, 1089-98. c) A. Tirella, A. Orsini, G. Vozzi, A. Ahluwalia *Biofabrication* **2009**, *1*, 045002. d) M. Mariani, F. Rosatini, G. Vozzi, A. Previti, A. Ahluwalia, *Tissue Eng.* **2006**, *12*, 547-57.

(7) T. H. Ang, F.S.A. Sultana, D. W. Hutmacher, Y. S. Wong, J. Y. H. Fuh, X. M. Mo, H. T. Loth, E. Burdet, S.H. Teoh, *Mat. Sci. Eng. C Bio S* **2002**, *20*, 35-42.

(8) a) R. Landers, A. Pfister, U. Huebner, H. John, R. Schmelzeisen, R. Muelhaupt, *J. Mater. Sci.* **2002**, *37*, 3107–3116. b) R. Landers, U. Hubner, R. Schmelzeisen, R. Mulhaupt, *Biomaterials* **2002,** *23*, 4437–4447.

(9) E. Kang, G. S. Jeong, Y. Choi, K. H. Lee, A. Khademosseini, S.-H. Lee, *Nature Mat.* **2011**, *10*, 877-883.

(10) B. Lanfer, U. Freudenberg, R. Zimmermann, D. Stamov, V. Ko¨rber, C. Werner *Biomaterials* **2008**, *29*, 3888–3895.

(11) S. Ghosh, S. T. Parker, X. Wang, D. L. Kaplan, J. A. Lewis *Adv. Funct. Mater.* **2008**, *18*, 1883–1889.

(12) a) T. Andersen, J. E. Melvik, O. Gåserød, E. Alsberg, B. E. Christensen, *Biomacromolecules* **2012**, *13*, 3703-10. b) M. Dentini, G. Rinaldi, D. Risica, A. Barbetta, G. Skjåk-Bræk *Carbohydrate Polymers*, **2005**, *59*, 489–499. c) M. Dentini, G. Rinaldi, A. Barbetta, D. Risica, C. Anselmi, G. Skjåk-Bræk *Carbohydrate Polymers*, **2007**, *67*, 465–473. d) A. Barbetta, E. Barigelli, M. Dentini *Biomacromolecules* **200**9, *10,* 2328–2337.

(13) a) K. M. Yamada, E. Cukierman, *Cell*, **2007**, *130*, 601-10. b) K. L. Schmeichel, M. J. Bissell, *J. Cell. Sci.* **2003**, 116, 2377-88. c) F. Pampaloni, E. G. Reynaud, E. H. K. Stelzer, *Nat. Rev. Mol. Cell. Biol.* **2007**, *8*, 839-45.

(14) K. P. Kanebratt,T. B. Andersson, *Drug Metab. Dispos.* **2008**, *36*, 1444-52.

(15) a) A. Guillouzo, A. Corlu, C. Aninat, D. Glaise, F. Morel, C. Guguen-Guillouzo, *Chem. Biol. Interact.* **2007**, 20,168(1):66-73. b) S. Anthérie, C. Chesné, R. Li, C. Guguen-Guillouzo, G. Guillouzo, *Toxicol in Vitro* **2012**, *26*, 1278–1285.

(16) a) S.B. Leite, I. Wilk-Zasadna, J. M. Zaldivar, E. Airola, M. A. Reis-Fernandes, M Mennecozzi, C. G. Guillouzo, C. Chesne, C. Guillou, P. M. Alves, S. Coecke, *Toxicological Sciences* **2012**, *130*, 106–116. b) P. Gunness, D. Mueller, V. Shevchenko, E. Heinzle, M. Ingelman-Sundberg, F. Noor, *Toxicol. Sci.* **2013**, 133, 67-78. c) M. Yamada, R. Utoh, K. Ohashi, K. Tatsumi, M. Yamato, T. Okano, M. Seki, *Biomaterials* **2012**, *33*, 8304-8315.

(17) A. Stampella, A. Papi, G. Rizzitelli, M. Costantini, C. Colosi, A. Barbetta, M. Massimi, L. Conti Devirgiliis, M. Dentini, *J. Mater. Chem.* B **2013**, *1*, 3083-3098.

(18) M. A. LeRoux, F. Guilak, L. A. Setton, *J. Biomed. Mater. Res.* **1999**, *47*, 46-53.

(19) M. Rinaudo, *Progress in Polymer Science* **2006**, *31*, 603-670.

(20) T. Dai, M. Tanaka, Y. Y. Huang, M. R. Hamblin, *Expert review of anti-infective therapy* **2011**, *9*, 857-879.

(21) N. Iwasaki, S.-T. Yamane, T. Majima, Y. Kasahara, A. Minami, K. Harada, S. Nonaka, N. Maekawa, H. Tamura, S. Tokura, M. Shiono, K. Monde, S.-I. Nishimura, *Biomacromolecules* **2004**, *5*, 828-33.

(22) H. Chen, W. Ouyang, M. Jones, C. Martoni, T. Haque, R. Cohen, S. Prakash, *Cell Biochem. Biophys.* **2006**, 47, 159-167.

(23) F. L. Mi, H. W. Sung, S. S. Shyu, *J. Polym. Sci. Part A-Polym. Chem.* **2000**, *38*, 2804-2814.

(24) Mi, F. L. *Biomacromolecules* **2005**, *6*, 975-987.

(25) S. Fujikawa, S. Nakamura, K. Koga, *Agric. Biol. Chem.* **1988**, *52*, 869-870.

(26) a) A. Bartkowiak, D. Hunkeler, *Chem. Mater.* **1999**, *11*, 2486- 92. b) O. Gaserod, O. Smidsrod, G. Skjak-Braek, *Biomaterials* **1998**, *19*, 1815-1825.

(27) a) A. Barbetta, A. Carrino, M. Costantini, M. Dentini *Soft Matter*, **2010**, *6*, 5213-5224. b) A. Barbetta, G. Rizzitelli, R. Bedini, R. Pecci, M. Dentini *Soft Matter*, **2010**, *6*, 1785–1792. c) I. Chimenti, G. Rizzitelli, R. Gaetani, F. Angelici, V. Ionta, E. Forte, G. Frati, O. Schussler, A. Barbetta, E. Messina, M. Dentini, A. Giacomello, *Biomaterials*, **2011**, *32*, 9271-9281.

(28) F-L. Mi, H-W. Sung, S-S. Shyu, *J Polym Sci Part A: Polym Chem.* **2000**, *38*, 2804-2814.

(29) K. Zhang, Y. Qian, H. Wang, L. Fan, C. Huang, A. Yin, X. Mo, *J Biomed. Mater. Res. A.* **2010**, *95A*, 870-881.

(30) G. Lawrie, I. Keen, B. Drew, A. Chandler-Temple, L. Rintoul, P. Fredericks, L. Grøndahl, *Biomacromolecules* **2007**, *8*, 2533-2541.

(31) J. Friedrich, C. Seidel, R. Ebner, L. A. Kunz-Schughart, *Nat. Protoc.* **2009**, *4*, 309-24.

(32) a) M.R. McGill, H.M. Yan, A. Ramachandran, G. J. Murray, D. E. Rollins, H. Jaeschke, *Hepatology* **2011**, *53*, 974-82. b) M. De Colli, M. Massimi, A. Barbetta, B. Di Rosario, S. Nardecchia L. Conti Devirgiliis, M. Dentini, *Biomed. Mater.* **2012**, *7*, 1-13.

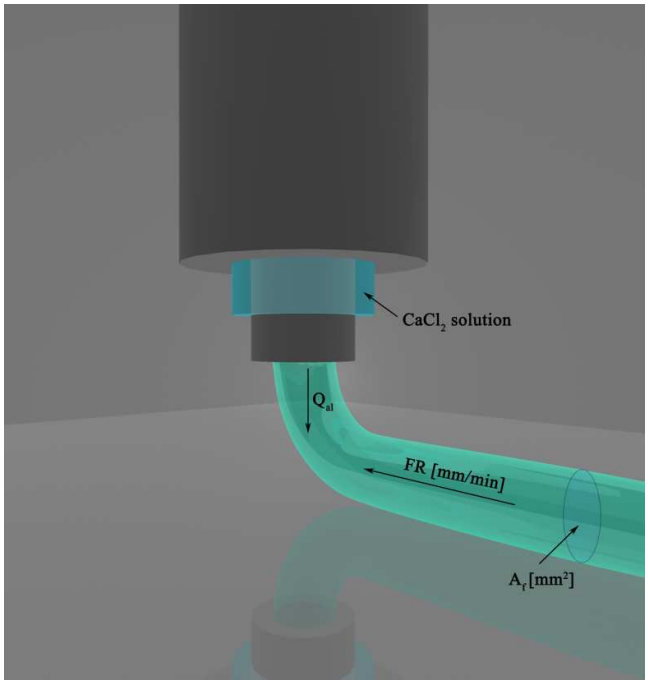

Figure 1. Scheme of the fiber extrusion process and representation of the physical parameters responsible in defining the fiber diameter.

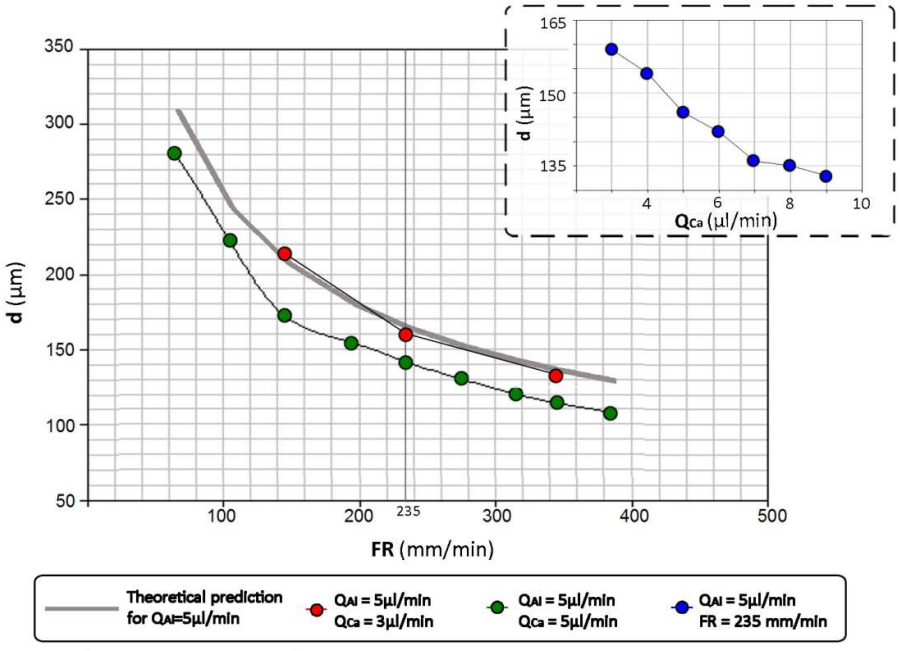

Figure 2. Dependence of fiber diameter on the speed of movement of the extruder (*FR*) and (insert) on the outer flow rate of $CaCl_2$ solution (Q_{Ca}) for constant alginate flow rate and for a given value of *FR*, (Q_{Al} = 5µl/min). The internal diameter of the inner needle is 260 µm, the internal diameter of the external needle is 690 µm.

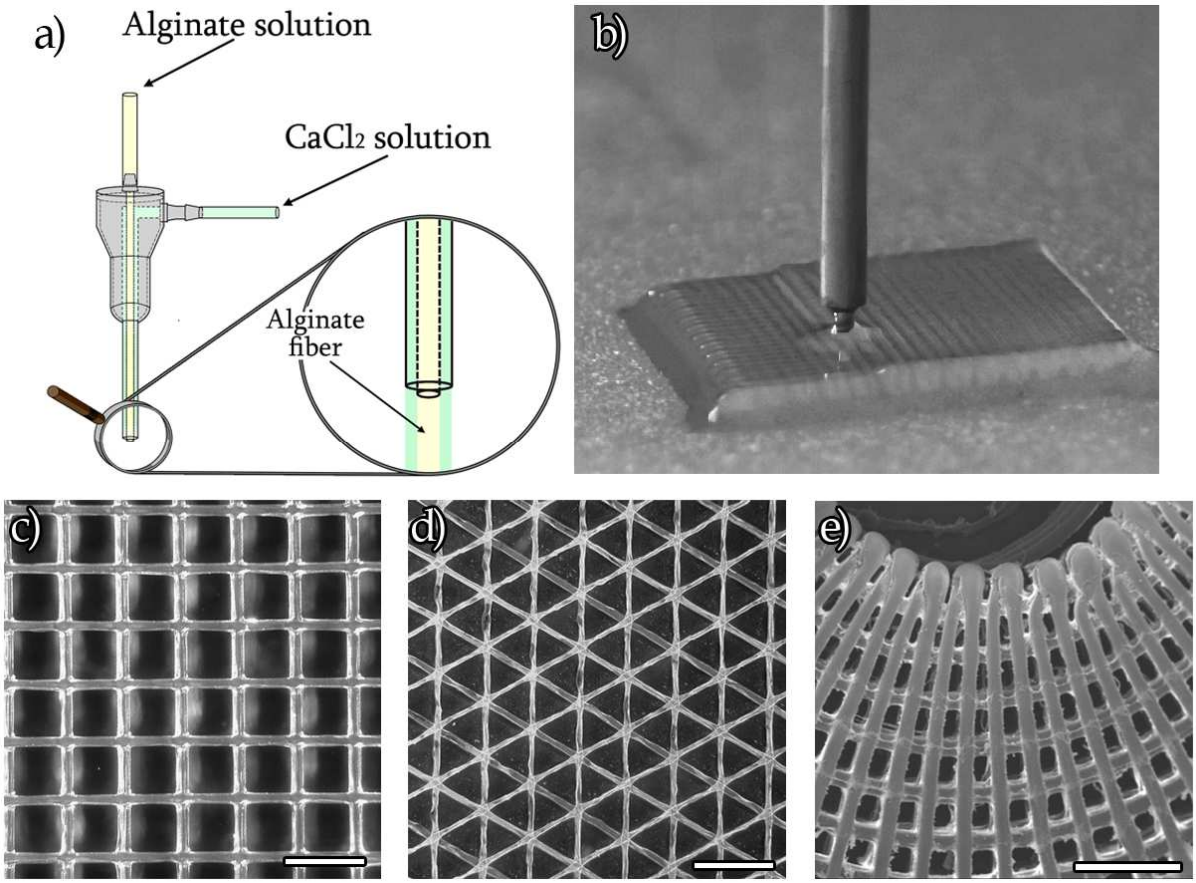

Figure 3. a) Schematic representation of the coaxial needles system for the extrusion of alginate fibers. b) Photograph of the 3D Fiber Deposition system during scaffold production. c,d,e) Optical micrographs of printed structures with c) squared, d) hexagonal and e) radial patterns of fibers. Scale bars: 500μm.

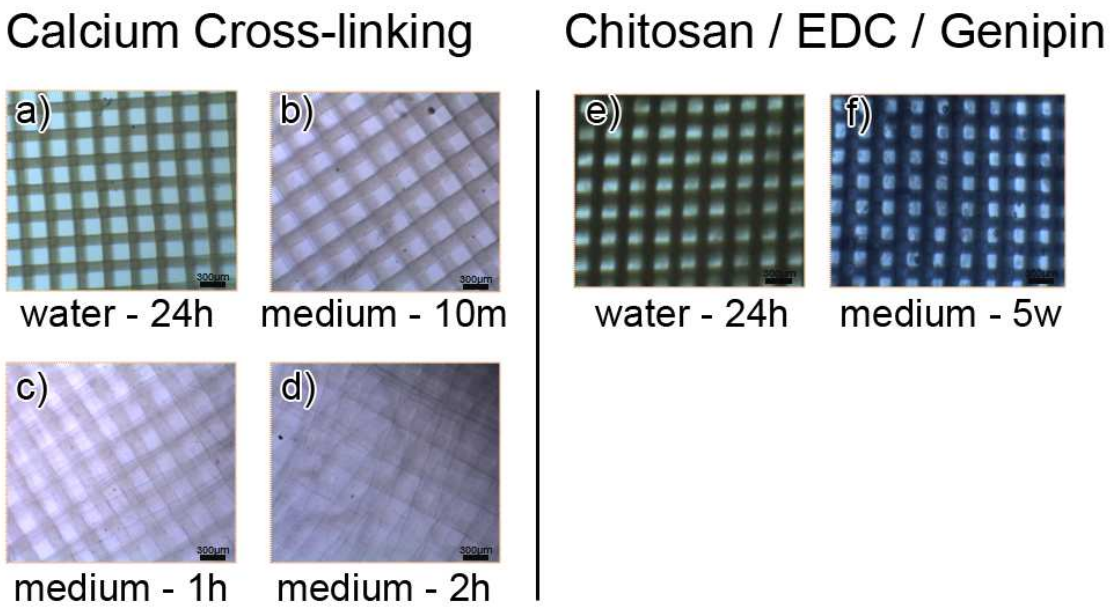

Figure 4. Optical micrographs of ionically cross-linked alginate scaffolds (a,b,c,d) and chitosan coated chemically cross-linked alginate scaffolds (e,f) in water (a,e) and in RPMI-1640 cell culture medium (b,c,d,f) at different soaking times (a,e: 24 hours; b: 10 minutes; c: 1 hour; d: 2 hours; f: 5 weeks).

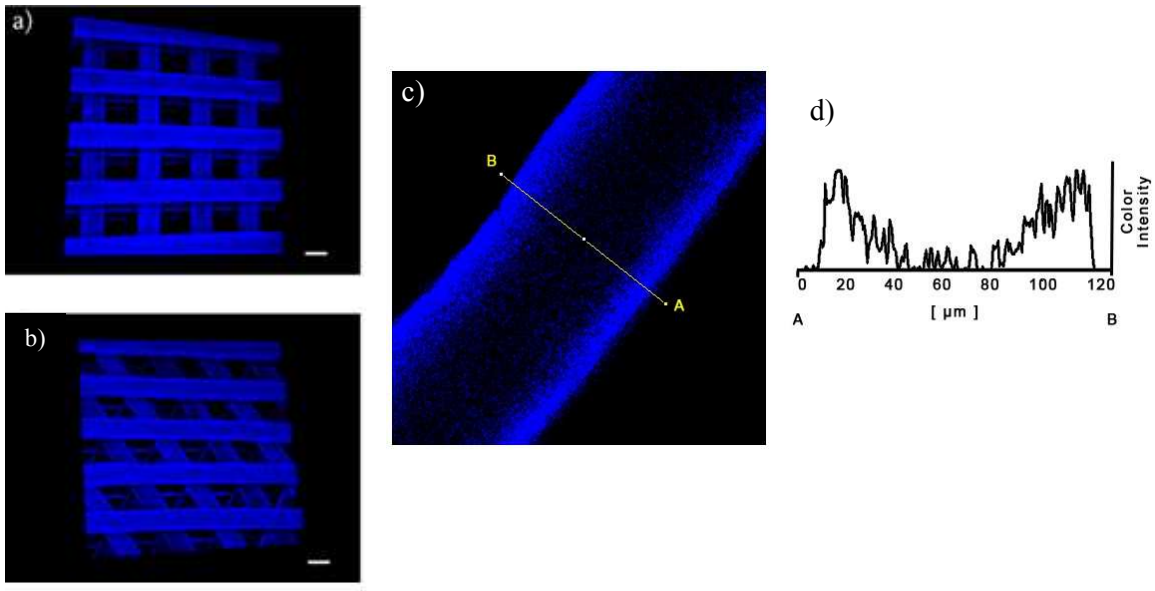

Figure 5. Confocal microscopy image of squared (a), hexagonal (b) scaffolds and c) of a section of a fiber. Scaffolds were coated with chitosan and cross-linked with EDC and genipin. Scale bars: 100 µm. d) plot of fiber color intensity profile for the segment A-B (obtained with ImageJ software). Blue light emission from the scaffolds/fiber is due to the chitosan/genipin complex.

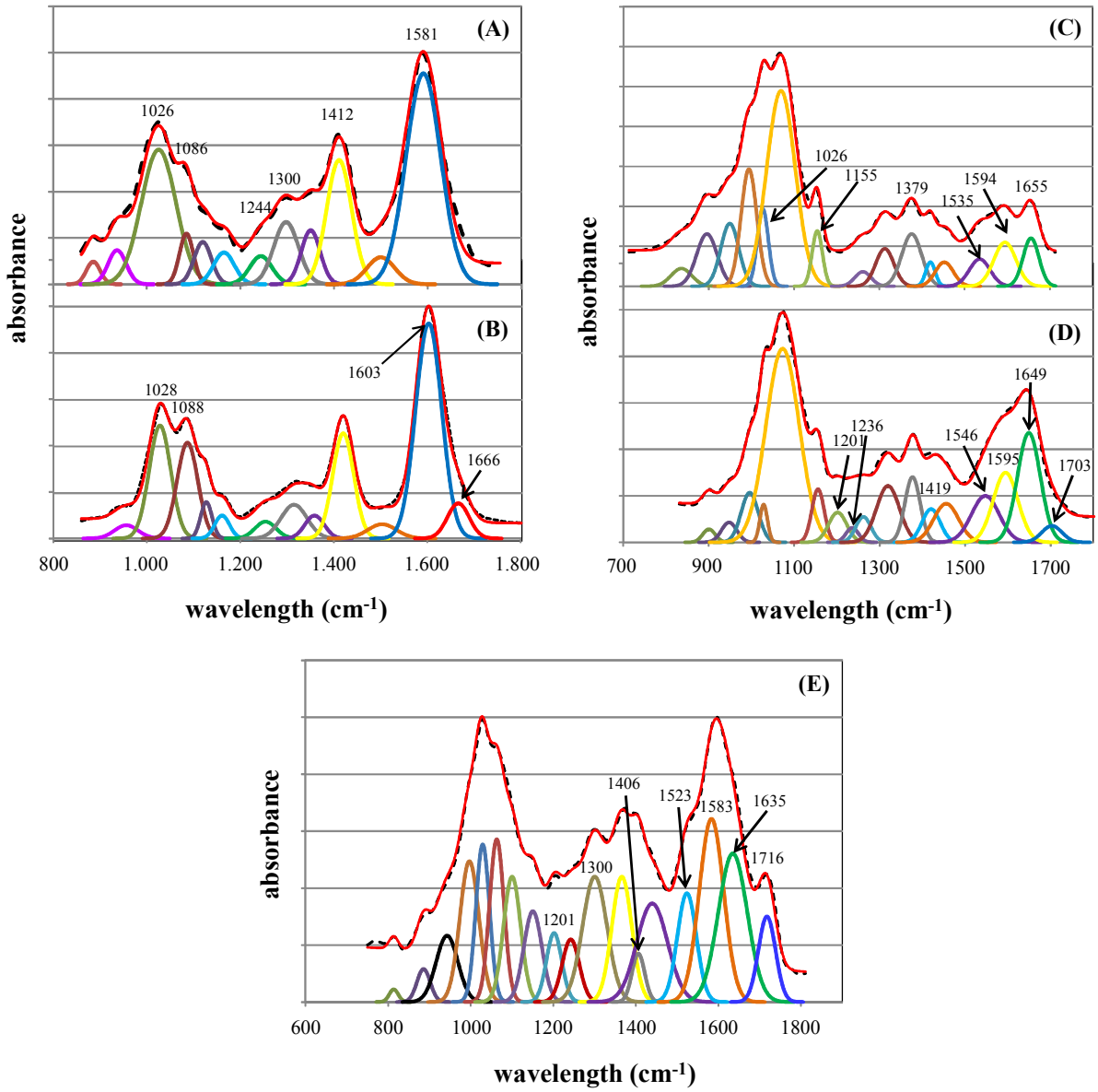

Figure 6. FTIR spectra of: (A) Ca^{2+}-alginate printed scaffold; (B) Ca^{2+}-alginate printed scaffold cross-linked with EDC; (C) chitosan; (D) chitosan scaffold obtained by gas-foaming and cross-linked with genipin; (E) printed scaffold of alginate coated with chitosan cross-linked with EDC and genipin.

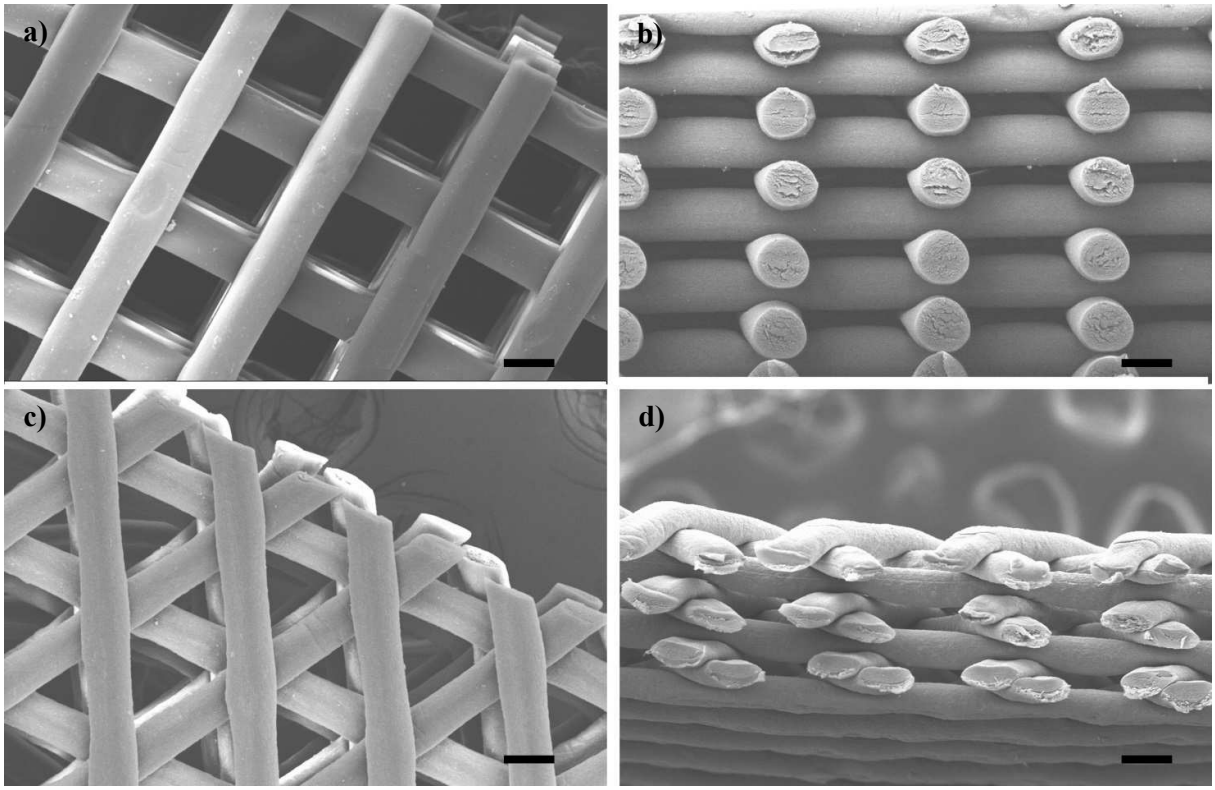

Figure 7. SEM micrographs of squared (a,b) and hexagonal (c,d) alginate scaffolds coated with chitosan and cross-linked with EDC and genipin. Scale bars: 100 μm.

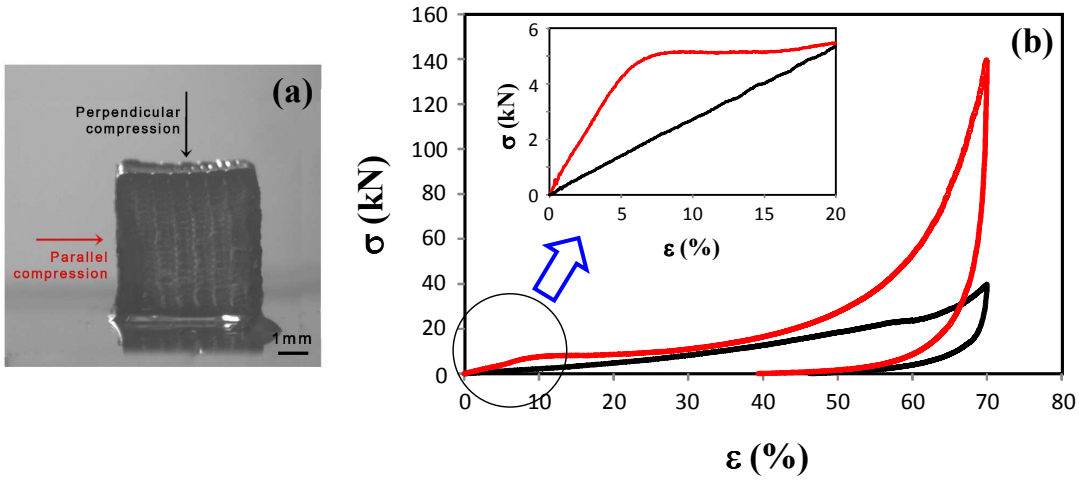

Figure 8. (a) Image of a scaffold sample used in compression tests. Arrows indicate the directions of the applied compression. (b) compressive stress (σ)-strain (ε) curves of Alg.Chit$_s$ determined in a direction perpendicular (black line) and parallel to the deposition plane (red line). In the insert, enlarged view of the portion of the curves in the range of strain 0-20% are shown.

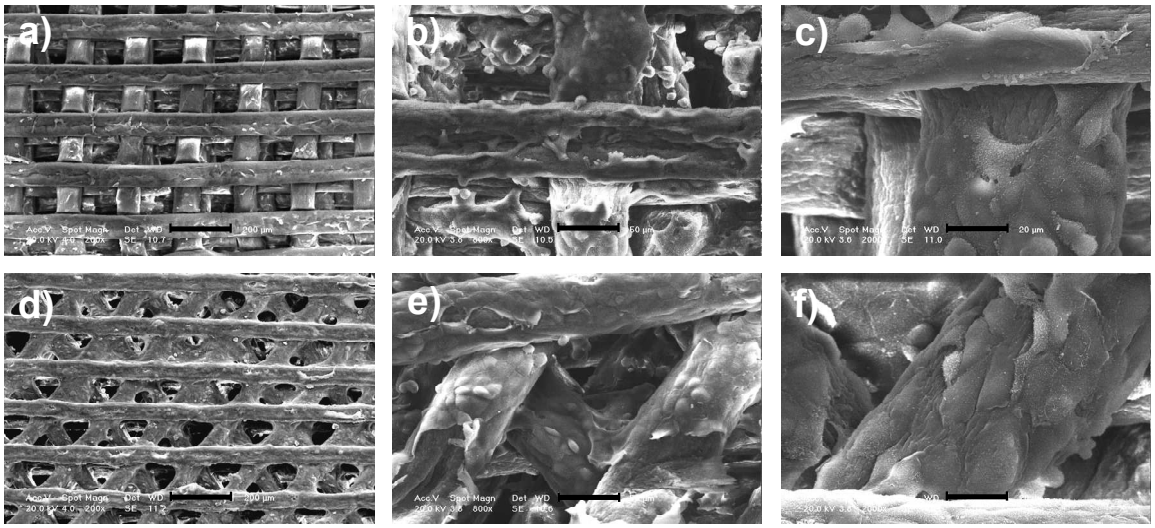

Figure 9. Scanning electron micrographs at different magnifications of HepaRG cells cultured for 6 (a, b, d, e) and 9 days (c, f) on squared (a, b, c) or hexagonal (d, e, f) chitosan-coated alginate scaffolds. A homogeneous distribution of cells and a high level of adhesion to the fibers are observed within both kind of scaffolds. Scale bars: a) and d) 200 μm; b) and e) 50 μm; c) and f) 20 μm.

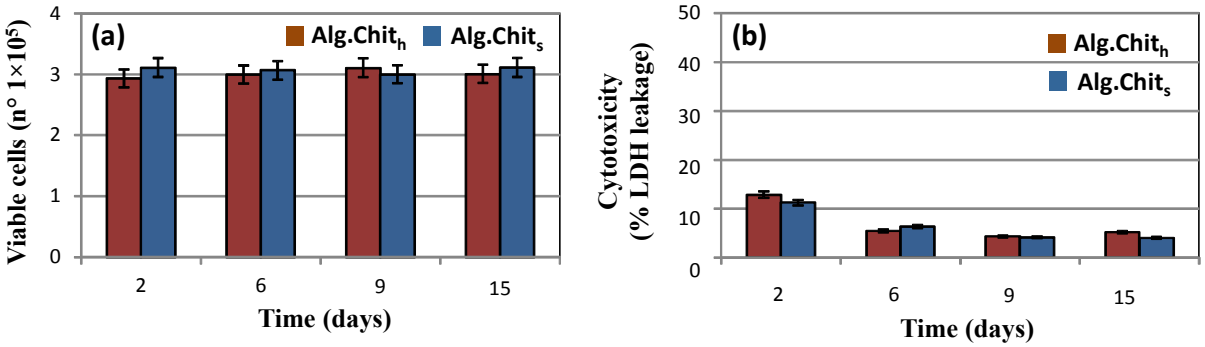

Figure 10. Viability (a) and cytotoxicity (b) assays of HepaRG cultured on hexagonal (Alg-Chit$_h$) or squared (Alg-Chit$_s$) chitosan-coated alginate scaffolds at 2, 6, 9 and 15 days. Results are the mean ± SD of at least three different experiments done in triplicate.

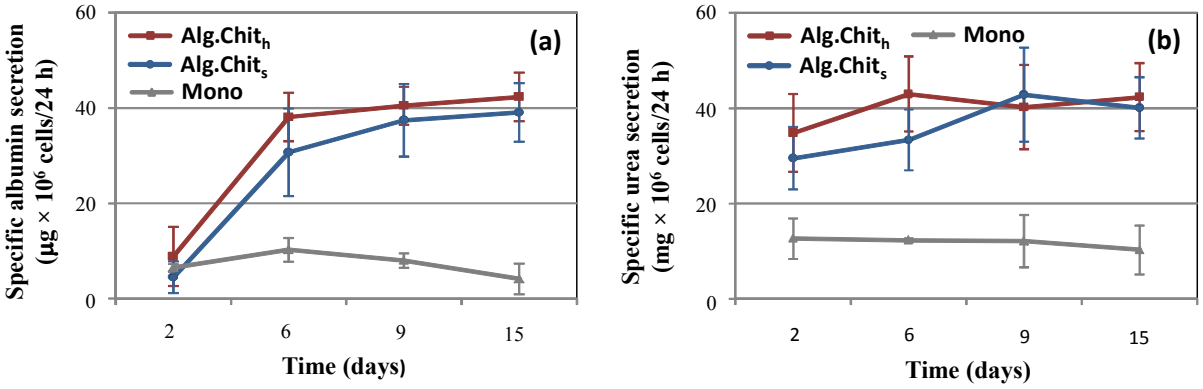

Figure 11. Albumin secretion (a) and urea production (b) from HepaRG cultured on hexagonal (Alg-Chit$_h$) or squared (Alg-Chit$_s$) chitosan-coated alginate scaffolds or in monolayer (Mono) at 2, 6, 9 and 15 days. At each time point, rates were normalized to the number of cells obtained by MTS assay and expressed as µg per 10^5 cells per 24h. Results are the mean ± SD of at least three different experiments done in triplicate.

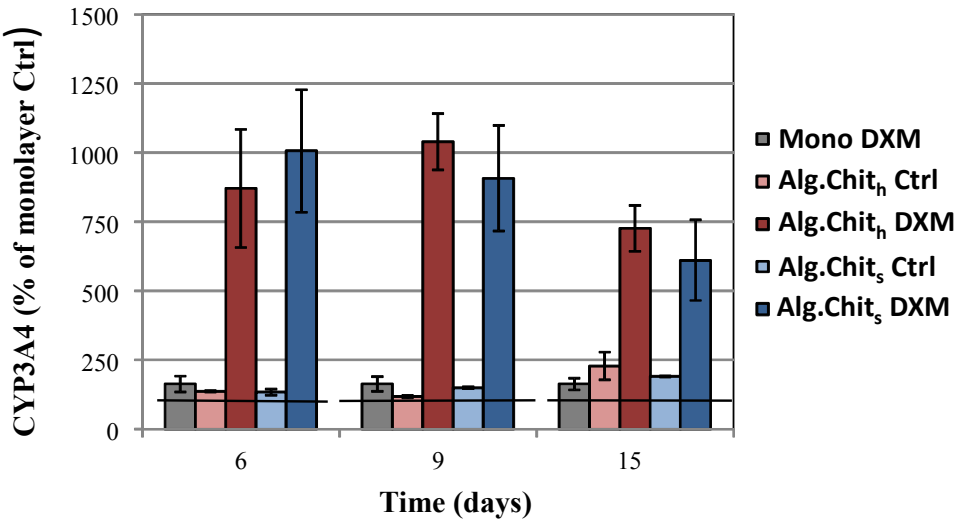

Figure 12. CYP3A4 activity, in absence or presence of the inductor DXM 10^{-4} M , in HepaRG cells cultured on hexagonal (Alg-Chit$_h$) or squared (Alg-Chit$_s$) chitosan-coated alginate scaffolds or in monolayer (Mono), at 6, 9 and 15 days. Values are reported as percentage of monolayer control, considered as 100% (black continuous line). Results are the mean ± SD of at least three different experiments done in triplicate.

Table 1. Young moduli of the printed scaffolds characterized by a square and hexagonal geometry determined according to a direction perpendicular ($E_{\perp}$) and parallel ($E_{\parallel}$) to the deposition plane.

Sample	$E_{\perp}$ (kPa)	$E_{\parallel}$(kPa)	***Nominal Porosity***[a]
Alg.Chit$_s$	23.3±4.2	77.2±7.2	66.6
Alg.Chit$_h$	25.7±3.8	51.3±6.4	66.3

[a]Porosity was calculated from the scaffold computer model by using an algorithm developed in Visual Basic.

TABLE OF CONTENT

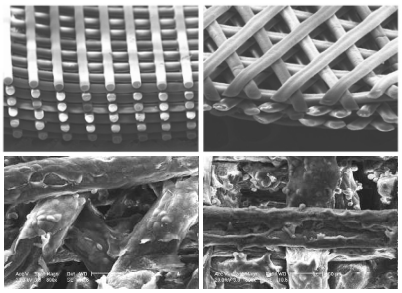

A novel dispensing system based on two coaxial needles is used to fabricate three dimensional, periodic scaffolds by rapid prototyping.